Determination of roughness correlations in multilayer films for x-ray mirrors

D. E. Savage, J. Kleiner, N. Schimke, Y.-H. Phang, T. Jankowski, J. Jacobs, R. Kariotis, and M. G. Lagally
Department of Materials Science and Engineering, University of Wisconsin-Madison, Madison, Wisconsin 53706

(Received 25 May 1990; accepted for publication 8 October 1990)

Interfacial roughness in multilayer films may be random or correlated, i.e., replicated from layer to layer. It is shown that these can be separated and quantified using x-ray diffraction rocking curves and a straightforward analysis. The lateral correlation length along the interfaces can additionally be determined. A quantitative evaluation for W/C multilayers shows that correlated roughness contributes significantly to the total roughness, even at length scales that are surprisingly short, of the order 2–6 nm.

I. INTRODUCTION

Artificial multilayered composite structures have a range of unique optical, mechanical, and electrical properties. Many of these properties result directly from the presence of a deliberately engineered one-dimensional lattice of alternate layers of different materials. As a consequence, the extent to which a multilayer structure exhibits these properties depends on the structural perfection of the superlattice. This statement is particularly true for optical and electronic properties, and specifically for the quality of soft x-ray optical elements. For these it is well known that interfacial roughness leads to a loss of specular reflectivity,[1] which is detrimental in both imaging and spectroscopy applications. This loss of specular reflectivity appears as an increase in the diffusely scattered radiation, leading to a loss of contrast in imaging systems.[2]

In general, multilayer structures, no matter what deposition technique is used, will not be perfect. There are a number of possible causes. For example, substrate roughness may be replicated by the growing film. If there is insufficient lateral mobility of adatoms, surface roughness and hence interfacial roughness will increase with the amount of material deposited.[3] Even for perfectly epitaxial systems grown under conditions of high mobility, a statistical surface roughness results because of the finite deposition rate.[4] Other complications may occur, including interdiffusion and chemical reaction at the interfaces. The identification of the nature of interfacial roughness is the first step in determining its cause and thus to developing procedures for its elimination.

In this paper we present results of a study of interfacial roughness in multilayer W/C soft x-ray mirrors whose aim is to distinguish between interfacial roughness that is correlated between layers and roughness that is random. By "correlated roughness" we mean excursions from the mean interface plane that are replicated from interface to interface in the multilayer stack. The fact that correlated roughness may occur in multilayer films used for visible-light optical coatings has long been recognized.[5–7] This large-scale figure error results from macroscopic digs and scratches on the substrate that are replicated by the film. Similar roughness correlations may also occur in soft x-ray multilayers, but here much finer-length-scale roughness, on the order of the x-ray wavelength, must be considered. Recent work by Zmek *et al.*[8,9] has stressed the detrimental effects of correlated roughness on x-ray imaging applications. They have suggested that the degree of roughness correlation depends on its lateral length scale, with the correlation becoming random at "short" lengths. Indirect evidence that large-scale substrate roughness can be propagated through soft x-ray multilayer mirrors has been obtained from high-resolution diffraction experiments.[10,11] It was found that the average slope error (long-wavelength waviness) measured on bare substrates was similar to that present in the multilayers and on their surfaces. A second demonstration that a correlation of large-scale roughness occurs is that multilayer diffraction gratings can be produced by using conventional optical diffraction gratings as substrates.[12–14] To our knowledge, no study has explored roughness correlations in soft x-ray multilayer mirrors quantitatively, determining their contribution to the total roughness. In addition, we believe that the possibility of the existence of fine-scale roughness correlations has not been adequately addressed.

We have developed a procedure to obtain directly the amount of correlated interfacial roughness present in multilayered films and the lateral wavelength of this roughness. To do this, we perform detailed x-ray diffraction measurements using Cu$K\alpha$ radiation. We measure the specular and diffuse components of the reflected radiation to determine separately the total interfacial roughness and the component due to roughness replicated from layer to layer, i.e., correlated in some manner with the substrate or due to a growth front effect that gives correlation in the film morphology. Additionally, we estimate lateral correlation lengths of the replicated roughness. We show that a considerable portion of the total interfacial roughness arises from correlated roughness. The mean wavelength of these correlations can be of such a magnitude as to be a significant factor in the design of x-ray optics and certainly is in the mirrors we have studied.

We begin, in the next section, with a review of relevant x-ray diffraction theory to outline the problem we are attacking. We will precisely define what we mean by correlated and uncorrelated roughness, and by lateral correlation length. In the following sections we describe the experiments used to

 0021-8979/91/031411-14$03.00

extract roughness and analyze data from samples grown with varying numbers of layers as well as grown on different types of substrates. We conclude that fine (nano)-scale roughness correlations make a significant contribution to the total roughness on all films measured, many of which are at the state of the art in x-ray mirror technology.

II. REVIEW OF THEORY OF SCATTERING FROM SURFACES, INTERFACES, AND MULTILAYER STRUCTURES

An extensive literature deals with the scattering of electromagnetic radiation (both visible and x-ray wavelengths) from nonideal surfaces and interfaces, in which the loss of specular reflectivity that is a consequence of surface or interfacial disorder is measured or calculated. In general, in these papers a mean roughness is obtained.[1,5-7,15-20] To extract the mean surface or interfacial roughness from a reflectivity experiment, the reduction of the specular reflectivity relative to that of a perfect mirror is modeled. If the distribution of heights of one or the other material at each interface is assumed to be a Gaussian and the average interfacial roughness is the same for each interface, then the specular reflectivity, I_{spec}, can be written approximately as

$$I_{\text{spec}} = I_0 \exp(-S_z^2\sigma^2), \tag{1}$$

where I_0 is the reflectivity of the perfect mirror, S_z is the perpendicular component of the momentum transfer vector, and σ is the rms roughness. Since no mirror is perfect, the value of I_0 can not be obtained through measurement and so can only be obtained from a dynamical calculation using Fresnel diffraction theory[21] or equivalently from the Ewald–von Laue dynamical diffraction theory.[22] The exponential has the effect of attenuating the reflectivity as either the roughness or the perpendicular component of the momentum transfer vector (i.e., the diffraction order) is increased. This approach is analogous to the treatment of the dynamic Debye–Waller factor[22] resulting from thermal vibrations, except that here the disorder is frozen in. Consequently the exponential in Eq. (1) has been called the static Debye–Waller factor. Equation (1) is the result of a kinematic scattering analysis and is independent of how the roughness is correlated from layer to layer. When multiple scattering is included the correlation of roughness must be specified. If roughness is assumed to be uncorrelated from layer to layer, Eq. (1) is altered somewhat.[16] If the roughness is assumed to be replicated perfectly the multiple-scattering analysis gives the same result as the kinematic and Eq. (1) is recovered.[5] Choosing a height distribution other than Gaussian will give rise to a different decay of the specular reflectivity as a function of S_z (diffraction order).[15,20] For the analysis presented in the remainder of the paper we retain the Gaussian approximation. We discuss the adequacy of this approximation for modeling specular reflectivity in Sec. IV. A.

There has been less work on measuring and modeling the diffusely scattered (nonspecular) radiation, particularly for soft x-rays. Models and measurements of the diffuse reflectivity of multilayer coatings for visible-light applications have been made.[5-7] For x-rays, the existing work deals chiefly with scattering from single rough surfaces.[17-19] In these types of studies the lateral correlation of the roughness, i.e., its lateral length scale, is determined from the angular profile of the diffuse component of the diffracted intensity. The intensity of the diffuse component integrated over a Brillouin zone equals the intensity removed from the specular direction. It is therefore also a measure of the total roughness. It can be written as[5]

$$\int_{\text{B.Z.}} I_{\text{diff}}\, dS = I_0\,[1 - \exp(-S_z^2\sigma^2)]. \tag{2}$$

The *shape* of the diffuse intensity reflects the scattering by the various Fourier components that the roughness represents and the strength of these components. These obviously in turn reflect correlations in roughness, i.e., the *lateral* height-height correlation function $C(X,Y)$, defined below.

For a single rough surface, the scattered intensity per unit area can be written as[18]

$$I(S) = I_0 \exp(-S_z^2\sigma^2)/S_z^2 \times \int\int dX\,dY \exp[S_z^2 C(X,Y)] \times \exp[-i(S_x X + S_y Y)], \tag{3}$$

where I_0 is the intensity per unit area of the incident beam and X,Y are the components of the lateral separation of two points on the surface. The correlation function $C(X,Y)$ is written

$$C(X,Y) = \langle z(x-X, y-Y) z(x,y) \rangle, \tag{4}$$

where $z(x,y)$ is the vertical displacement of the surface from its average height at the site defined by the lateral coordinates (x,y). Both Gaussian and exponential correlation functions have been used to model surface roughness (surface "finish").[5-7,17-19] More recently attempts to treat the rough surface as a fractal have given rise to other choices.[18,19] For an isotropic surface, the correlation function will depend only on the magnitude of the separation of the points X,Y and not on direction. We will discuss the relationship between the choice of the correlation function and a physical description of the interfacial roughness in Sec. IV. B 1.

Consider, as an example, the exponential correlation function

$$C(R) = \sigma^2 \exp(-|R|/\xi), \tag{5}$$

where $R = (X^2 + Y^2)^{1/2}$ and ξ is the lateral correlation length. One can insert $C(R)$ into Eq. (3) and simplify the problem to a one-dimensional one by integrating both sides of the equation over S_y. This integration is realized experimentally by detecting the scattered x rays with a sufficiently long slit. Information is thereby lost, of course, about the correlations in y. The term $\exp[S_z^2 C(X,0)]$ can be expanded and each term Fourier transformed analytically. The intensity can be separated into a sum of two terms, a delta function and a diffuse term,

$$I(S_x,S_z) = 2\pi I_0 (e^{-S_z^2\sigma^2})/S_z^2 \times\left[2\pi\delta(S_x) + \sum_{m=1}^{\infty} \frac{2\xi(S_z^2\sigma^2)m}{m(m!)} \times \frac{1}{(1+S_x^2\xi^2/m^2)}\right]. \quad (6)$$

For this example the diffuse term is a sum of Lorentzians, which converges rapidly for a sufficiently small $S_z\sigma$ product. The width of the diffuse term is inversely related to ξ and also depends on the magnitude of σ, the rms roughness, as more terms must be included for a larger σ. The area under the diffuse component depends only on σ, as exprected for a kinematic model. A similar analytic result can be obtained for a Gaussian correlation function, in which case the diffuse term is a sum of Gaussians. More complicated correlation functions can be used but the intensities can then be obtained only with numerical methods. The general trends of the effects of σ and ξ on the shape of the diffuse intensity will hold for the other choices of the correlation function as well. Thus, for a given σ, the peak intensity of the diffuse component will be greater for larger ξ, (i.e. longer-scale roughness) and the diffuse-peak width will be smaller. The peak intensity of the diffuse component will of course also increase for larger σ at constant ξ.

The question that now arises is what can be learned from the study of the diffuse reflectivity of a multilayer stack rather than of the single rough surface we have just considered? If the average layer spacing doesn't change throughout the thickness of the film, as expected for stable deposition conditions, then the diffraction of x rays from a stack of rough interfaces can be treated in a manner similar to thermal diffuse scattering in 3-d crystals.[22] The expected result is, as earlier, the sum of a sharp and a diffuse term. The first is the intensity scattered from the perfect crystal (but with a reduced magnitude) which arises because the average lattice spacing is maintained throughout the crystal. The diffuse intensity is due to scattering off the disorder; it has a shape that depends on the scatter-scatterer correlation in the direction measured. For multiple interfaces both lateral and vertical roughness correlations must be considered. Just as the shape of the diffuse intensity scattered from a single surface and measured in a direction parallel to that surface gives information on the lateral correlation of the surface roughness, the shape of the diffuse intensity scattered from a multilayer stack and measured parallel to the interfaces will give information on the lateral correlation of the interfacial roughness. Conversely, a measurement of the *vertical* distribution of the diffuse intensity (i.e., changing the energy or the angle of the incident radiation to move along S_z) will provide information about the vertical correlation of roughness from layer to layer.

It is straightforward to describe the results expected from scattering off a multilayer film for the special cases of vertically perfectly correlated roughness and vertically random roughness. The case of perfect correlation, i.e., substrate roughness replicated from layer to layer, has been treated by Eastman.[5] The result is simply the product of the intensity scattered by a single rough surface and the reflectivity of the perfect stack. In other words, the configuration of the replicated interface can be treated as an effective structure factor that can be factored out of the problem. Alternatively, for no vertical correlation, there is a random phase relation between the intensities diffusely scattered from each layer. The total intensity will be the incoherent sum of the intensities diffusely scattered from each layer plus the reduced specular reflectivity obtained from Eq. (1). Note that each layer may still individually have lateral correlations in roughness and hence produce diffuse scattering with a well defined intensity distribution in the S_x, S_y plane. The two results, vertically perfectly correlated and random roughness, are quite different and are illustrated schematically in Fig. 1. For perfect correlation, the diffuse intensity along S_z will be peaked at the Bragg conditions, $S_z = 2\pi n/d$. For vertically random roughness, the diffuse intensity will not be peaked, but will be spread out uniformly in S_z. The contribution of the diffuse intensity at the Bragg condition will then be weaker by a factor of $1/N$ compared with the diffuse intensity from layers with the same rms but perfectly correlated roughness, where N is the number of layer pairs.

A real multilayer film will have a vertical roughness correlation somewhere between these two limiting situations. It has long been expected that large-scale figure error, due to large-amplitude, low-frequency roughness in the substrate, is replicated by each layer deposited. In contrast, *high*-frequency roughness has generally been assumed to be uncorrelated[8,9,15,16] (with one exception[20]). The total interfacial roughness can formally be separated into parts that are correlated perfectly in z (like a perfect 3-d crystal) and uncorrelated (fluctuations away from the perfect crystal), i.e.,

$$\sigma_{\text{tot}}^2 = \sigma_c^2 + \sigma_u^2. \quad (7)$$

This can be demonstrated by considering the dependence on S_z of the reflectivity integrated over S_x, S_y. Doing so throws away information on correlations in the x and y directions and the intensity will depend only on correlations in Z, $C(0,0,Z)$. It will have maxima at the positions of the Bragg peaks and a diffuse intensity between peaks that is due to uncorrelated or partially correlated roughness. From Eq. (2), the integral of the diffuse reflectivity will have a value $I_0[1 - \exp(-S_z^2\sigma_u^2)]$. The specular reflectivity is the integral in S_z of the intensity over the Bragg peak minus the contribution of the uncorrelated diffuse intensity and equals $I_0[\exp(-S_z^2\sigma_u^2)]$. This intensity is then the sum of the true specular reflectivity and the value of the diffuse term due to the vertically correlated roughness at $S_x = S_y = 0$. Thus, the correlated diffuse reflectivity can be written as

$$I_{\text{diff}}(\text{correlated}) = I_0 \exp(-S_z^2\sigma_u^2) \times[1 - \exp(-S_z^2\sigma_c^2)], \quad (8)$$

while the true specular reflectivity can be written as

$$I_{\text{spec}} = I_0 \exp[-S_z^2(\sigma_u^2 + \sigma_c^2)]. \quad (9)$$

Equations (8) and (9) lead directly to the result that the ratio of the true specular reflectivity to the integral of the correlated diffuse reflectivity depends only on σ_c and suggests a method for separating out the contribution of each

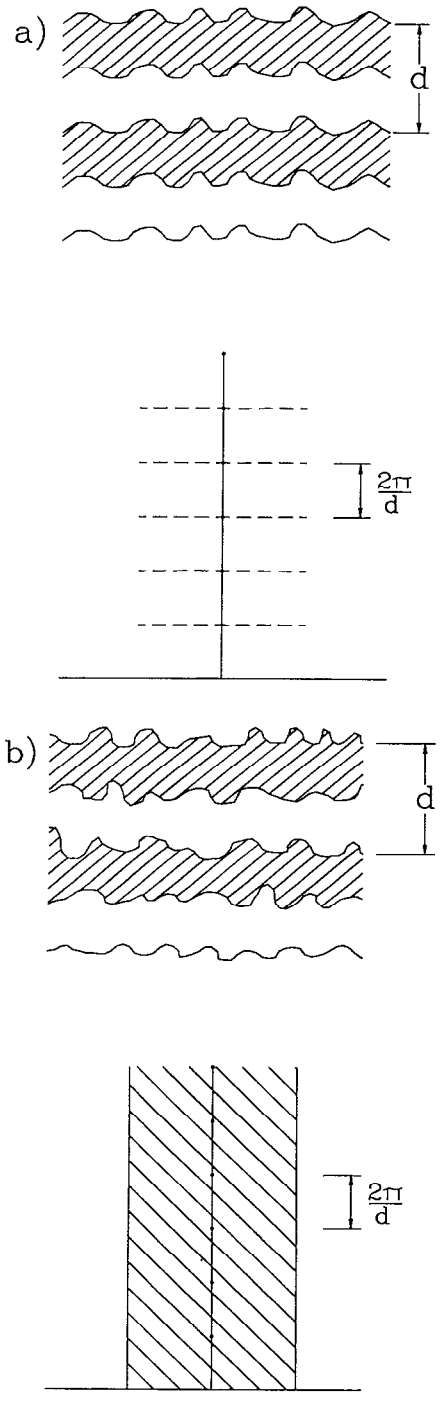

FIG. 1. A schematic view of correlated and uncorrelated interfacial roughness and corresponding reciprocal lattices. (a) correlated perfectly from layer to layer and (b) uncorrelated from layer to layer. The reciprocal-space representation for each situation is shown in the lower panels. Perfect correlation concentrates the diffuse intensity in S_x,S_y planes centered at $S_z = 2\pi n/d$, the Bragg conditions. For uncorrelated roughness diffuse intensity is spread in all directions.

kind of roughness. The total rms roughness can be obtained by fitting a theoretical calculation to a measurement of the intensity of the specular reflection as a function of S_z. Fitting the shape of the reflected peak in S_x, S_y with the models for the single surface will give the rms roughness and lateral correlation length of the vertically correlated disorder. It should be noted that the specular peak intensity must be corrected for the contribution of the diffuse intensity arising from both correlated and uncorrelated roughness to obtain a true rms roughness. Similarly, the diffuse intensity in the S_x, S_y plane at $S_z = 2\pi n/d$ (the Bragg conditions) must be corrected for the contribution of the intensity due to the uncorrelated roughness in order to obtain a true measure of the correlated roughness.

III. EXPERIMENT

A. Sample preparation

Multilayer films were deposited in a dc magnetron sputter deposition system with a base pressure of 3×10^{-7} Torr, shown schematically in Fig. 2. Substrates were loaded onto a turntable and passed alternately over carbon and tungsten sources. The sputtering gas was Ar with a typical value of the partial pressure during deposition of 5 mTorr. Deposition is nominally at room temperature, although the substrates may reach 100 °C for some deposition conditions. The resultant growth rates, with a stationary table, for C and W were 0.9 and 1.8 Å/s, respectively. Layer thicknesses were controlled by varying the table speed. The nominal bilayer spacing, d, was chosen to be 40 Å with C and W layers of approximately equal thickness. Such a layer spacing is appropriate

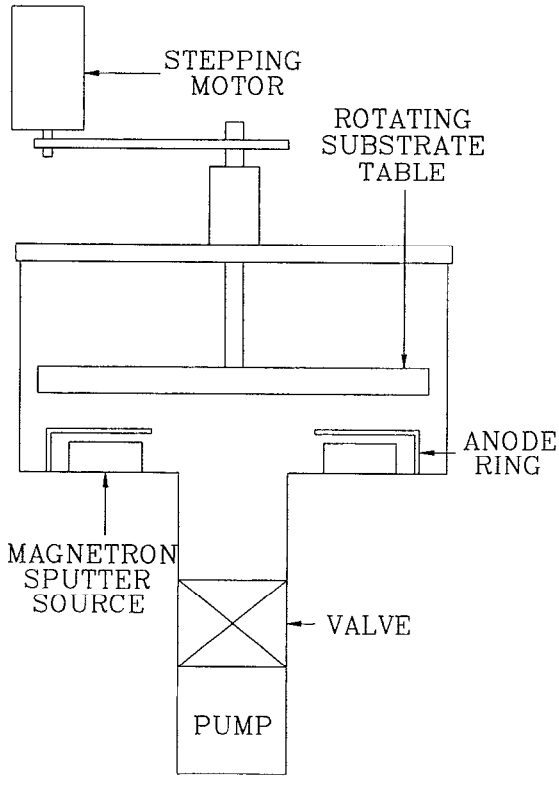

FIG. 2. A schematic view of the deposition system showing the tungsten and carbon dc magnetron sputtering sources and the substrate turntable. The turntable is driven by a computer controlled stepper motor coupled to a rotary ferrofluidic feedthrough.

for near-normal-incidence applications involving shorter wavelength x rays in the soft x-ray range. Smaller layer spacings lead to a degradation of mirror quality that is generally ascribed to the increased importance of the part of each layer that is rough as the films get thinner. The ratio of film thicknesses, $\Gamma = t_W/(t_W + t_C) = 1/2$, was chosen in order to maximize the integral of the first-order reflectivity while minimizing the second.

Forty, sixty, and eighty-layer-pair mirrors were deposited on Si(100) wafer substrates. Forty-layer pair films were also deposited on Suprasil silica substrates. Substrates were cleaned untra sonically in acetone and then methanol. More complex cleaning procedures, such as ones involving removal of the native oxide layer on the Si(100) substrates, always gave poorer results.

B. X-ray diffraction measurements

Measurements to distinguish correlated from uncorrelated roughness were made with a conventional two-circle x-ray diffractometer. The angle between the source and sample (ω) and the angle between source and detector (2θ) can be varied independently and are stepper motor controlled to an accuracy of 0.001°. The source is a Cu x-ray tube and the detector incorporates a graphite crystal monochromator set to detect Cu$K\alpha$ radiation. The source slits subtend an angle of 0.03° with respect to the source within the plane of diffraction and the detector aperture subtends an angle of 0.01° with respect to the source. The source slit height subtends an angle of 3.5° with respect to the sample while the exit slit height subtends an angle of 2.08°.

To obtain the absolute reflectivity of the layer stack at the Cu$K\alpha$ wavelength (1.54 Å), we made separate measurements of the incident and first-order reflected beams under the same power settings. For measurements of the weaker reflections, higher source power settings were used and overlapping scans at both settings were made to scale the reflectivity to the incident beam.

In order to separate correlated from uncorrelated roughness we must first determine the true specular reflectivity, i.e., we must subtract contributions of the diffuse intensity to the specular intensity. In addition, we want to determine how the diffuse reflectivity is distributed in reciprocal space. To do so, data were obtained in several different geometries as shown in Fig. 3. These various geometries map out the distribution of the scattered intensity in different cuts through reciprocal space necessary to separate out the types of roughness we described above. They are: (1) $(\theta,2\theta)$, (2) rocking curve, and (3) offset $(\theta,2\theta)$. In the $(\theta,2\theta)$ geometry, the specular reflectivity is measured as a function of the incident angle, producing a scan of the intensity integrated over the detector as a function of S_z. In the rocking curve geometry, 2θ is held fixed and ω is varied. Through the use of a narrow entrance slit to the detector, this type of measurement profiles the angular distribution of the scattered x rays in a cut perpendicular to the surface normal. Such a measurement allows one to separate out the value of the true specular reflection, which appears as an instrument-limited spike above a slowly varying diffuse background. Finally, in the offset $(\theta,2\theta)$ geometry, measurements are made with the crystal rotated a small fixed amount in order to profile the vertical distribution of the off-specular radiation I_{diff} vs S_z). This allows one to separate the intensity due to correlated roughness, which is confined

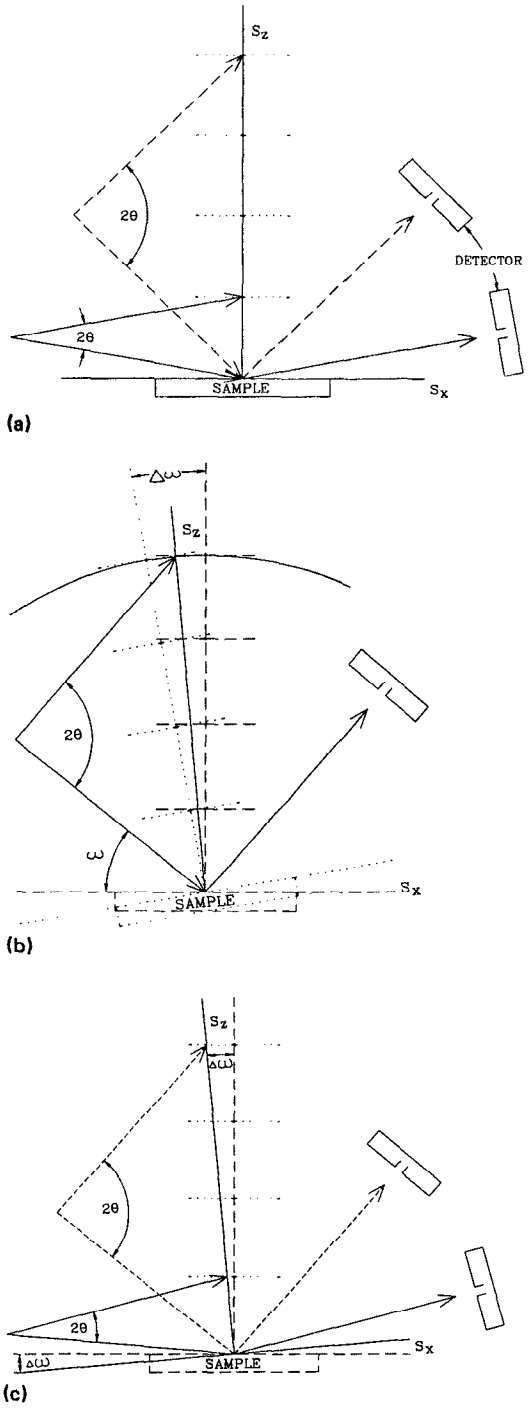

FIG. 3. Ewald constructions showing how the three different measurement geometries sample reciprocal space. (a) $(\theta, 2\theta)$ scan: diffracted intensity normal to the surface, $I(0,0,S_z)$, is collected; (b) rocking curve (I vs ω): by rocking the sample (i.e., fixing 2θ) and using a narrow detector aperture, a radial cut that approximates a cut in the S_x, S_y plane, $I(S_x, 0,$ const), is obtained; (c) offset $(\theta, 2\theta)$ scan: the crystal is tilted a small fixed amount and a conventional $(\theta, 2\theta)$ scan taken. Profiles of the diffuse intensity in a direction nearly normal to the sample surface are obtained. The figure is otherwise identical to (a).

to the S_x, S_y plane at the Bragg condition $S_z = 2\pi n/d$, from that due to the uncorrelated roughness.

The choice of the azimuthal direction of the incident x-rays was important because of long-range anisotropies in the grown films and because the incident x-ray beam is much higher than it is wide. The film thickness varied $\sim 10\%$ over the length of the sample (5 cm) in the radial direction of the rotating table, leading to a gradual variation of the bilayer spacing in that direction. Such a variation will appear in a $(\theta,2\theta)$ scan as an increase in the angular width of the reflected peak as a function of the diffraction order. This effect is observed when the incident azimuth is chosen along the tangential direction. In that case, the detector integrates the scattered intensity from an ~ 1 cm line on the sample along the radial direction. For the results we report here, the incident azimuth was chosen along the radial direction so that the exit slit integrates intensity along the tangential direction (a line of uniform d spacing) and no broadening of the diffracted peaks with order was observed.

IV. RESULTS AND ANALYSIS

A. Specular reflectivity

Examples of measured specular reflectivity [$(\theta,2\theta)$ curves] from 40-layer-pair mirrors grown on two different types of substrates are plotted in Fig. 4. The solid curves are the data and the dashed are calculated using the theory of Peterson *et al.*[16] Also shown, as solid triangles, are peak intensities from the rocking-curve measurements (see below) through the specular beam obtained at different values of 2θ with the contribution of the diffuse background subtracted. Mirrors grown on a polished Si(100) substrate exhibit a higher reflectivity and more diffraction orders than those grown on Suprasil silica, implying that the sample grown on the Si wafer has less disorder. This result can be quantified using model fits to data such as that shown in Fig. 4 in which $\sigma_{\rm tot}$ and Γ are free parameters. The calculated curves were obtained under the assumption that for a given film, the surface and all interfaces had the same degree of roughness. For the 40-layer pair film grown Si(100), the best fit gives $\sigma_{\rm tot} \cong 3.4$ Å. From the film grown on quartz $\sigma_{\rm tot} \cong 6.6$ Å.

In these measurements no distinction can be made between correlated and uncorrelated roughness. As was mentioned previously, kinematic diffraction theory predicts the static Debye–Waller factor reduction of the specular reflectivity independent of how the roughness is correlated. Dynamical-diffraction calculations of the specular reflectivity will depend on whether roughness is correlated, but the magnitude of the effect is small. To obtain information on the roughness correlations, other measurements, reported below in Sec. IV B, must be performed.

In order to examine the effect of film thickness on the total roughness, $(\theta,2\theta)$ scans were made for films consisting of different numbers of layer pairs deposited on Si(100) wafers. The results indicate no clear trend for the range of thicknesses we have so far investigated, although it appears that the roughness at first increases. Model fits to some of the data are summarized in Table I. The range of roughness values extracted from the fit for any one mirror arises because no single $\sigma_{\rm tot}$ could be found to fit the reflectivity for all orders. This appears to be a problem in careful attempts to fit $(\theta,2\theta)$ scans.[20] Either the intensity of the first order is overestimated or that of the highest orders is underestimated. Fitting the highest orders gives a lower limit to the total roughness but predicts a first-order reflectivity that is in some cases too high by as much as 50%. One possible origin of this discrepancy is that the sample depth being probed

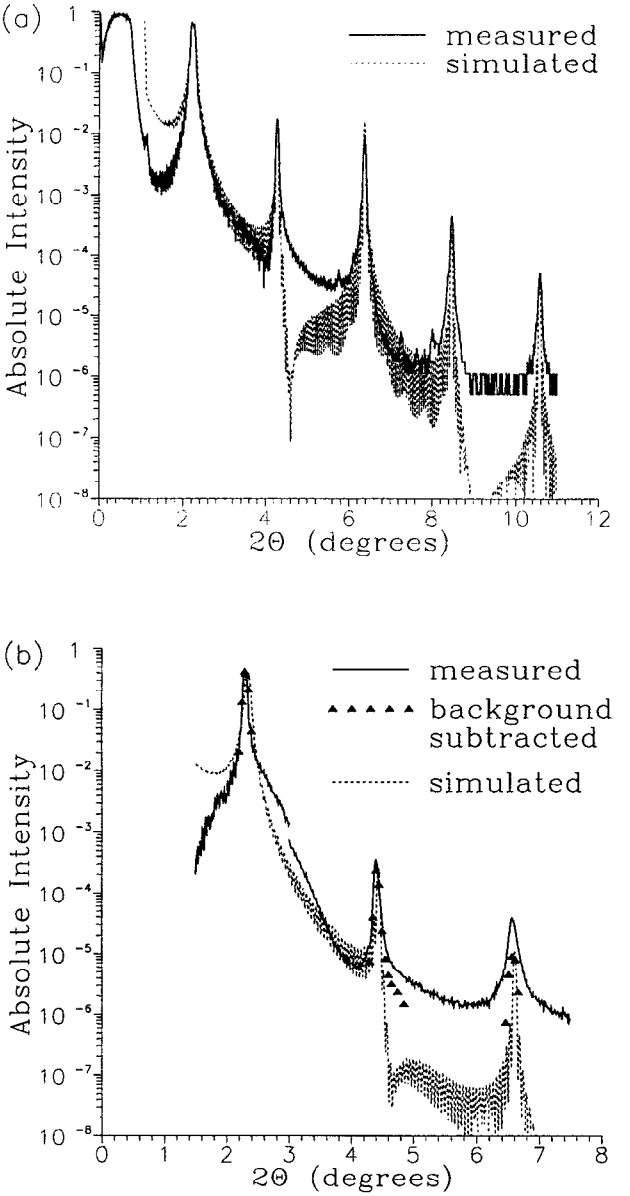

FIG. 4. Specular reflectivities obtained from 40 W/C layer pairs deposited on different substrates using the $(\theta, 2\theta)$ scan geometry. The data (solid curves) along with calculated fits (dashed curve) and the specular reflectivity after the contribution of the diffuse intensity in the specular direction was subtracted (solid triangles) are plotted. (a) Si(100) wafer substrate (solid line), with fit (dashed curve); first through fifth orders, using $\Gamma = 0.47$, $d = 41.9$ Å, and $\sigma_{\rm tot} = 3.4$ Å; (b) fused silica substrate (solid curve), first through third orders. The solid triangles give the intensity after the diffuse intensity due to interfacial roughness (Fig. 6) is subtracted. The dashed curve is a fit to these latter values, using $\Gamma = 0.48$, $d = 40.4$ Å, and $\sigma_{\rm tot} = 6.6$ Å.

TABLE I. Summary of the results of fitting the specular reflectivity [$(\theta,2\theta)$] curves. The total interfacial roughness, σ_{tot}, along with the bilayer period, d, and the fraction of the bilayer thickness that is tungsten, Γ, are shown for each sample. The large range of roughness values for the $N = 60$ and 80 layer-pair samples arises from the difficulty in fitting all orders with the same roughness value. The asterisked values are from fitting the first order preferentially.

Sample	d(Å)	Γ	σ_{tot} (Å)
Fused silica substrate			
$N = 40$	40.4	0.48	6.6 ∓ 0.2
Si (100) substrate			
$N = 40$	41.9	0.47	3.4 – 4.1*
$N = 60$	37.5	0.41	3.6 – 5.0*
$N = 80$	36.5	0.41	4.4 – 5.6*

varies with the angle of incidence, the probed depth being less at more grazing angles of incidence. Thus the value for σ obtained from fitting the first order reflects preferentially the interfacial roughness near a film's outer surface, while the value for σ obtained from fitting the higher orders represents more of an average interfacial roughness. The intensity of the first order then is attenuated preferentially either if roughness is increasing throughout the thickness of the film or, alternatively, if the surface roughness is much larger than the average. In either of these cases the value of σ obtained from fitting the higher orders is more representative of the average value for the bulk of the sample.

Another possibility for the discrepancy in fit between orders is that the assumption of a Gaussian distribution of interfacial heights is not correct. Other distributions, as outlined by Stearns,[15] were used to fit the decay of the specular reflectivity with order. The rms roughness values obtained from fitting the first order were in reasonable agreement with the values obtained with the Gaussian distribution. The fit to the higher orders with the other distributions was in general worse than with the Gaussian. This suggests that, while a function that we have not tried may fit the specular decay more closely than the Gaussian does, it is likely that the resultant roughness values will be similar to those obtained with the Gaussian.

B. Diffuse reflectivity

The total of the diffusely scattered intensity reflects the amount of roughness at the various interfaces while its distribution in reciprocal space reflects the degree of correlation present. We begin by presenting results that show that a significant amount of vertically correlated roughness is present on all samples and that its lateral correlation length is quite short. We will then quantify this observation with the use of the model presented earlier.

In Fig. 5(a) $(\theta,2\theta)$ curves taken in the specular geometry and with the sample rotated 0.5° off specular [offset $(\theta,2\theta)$ curves] are plotted for a 40-layer pair film grown on Si(100). In Fig. 5(b) a similar set of curves is plotted for a film grown on fused silica. The angular range covered in each scan contains the second and third orders. Note that in both data sets the relative contribution of the diffuse intensity (the dashed curves) increases with order, as expected from Eq. (2), and has essentially the same shape as the specular intensity. This peaking of the diffuse intensity in S_z at the Bragg condition implies that vertically correlated roughness is present. (Recall that for perfect vertical correlation of the roughness all the diffuse intensity is confined to the S_x, S_y plane at the Bragg condition $S_z = 2\pi n/d$.) The greater proportion of diffuse reflectivity in the total reflectivity for the films grown on fused silica is consistent with a larger total roughness and suggests a larger value of correlated roughness for this sample as well.

An estimate of the lateral length scale of the vertically

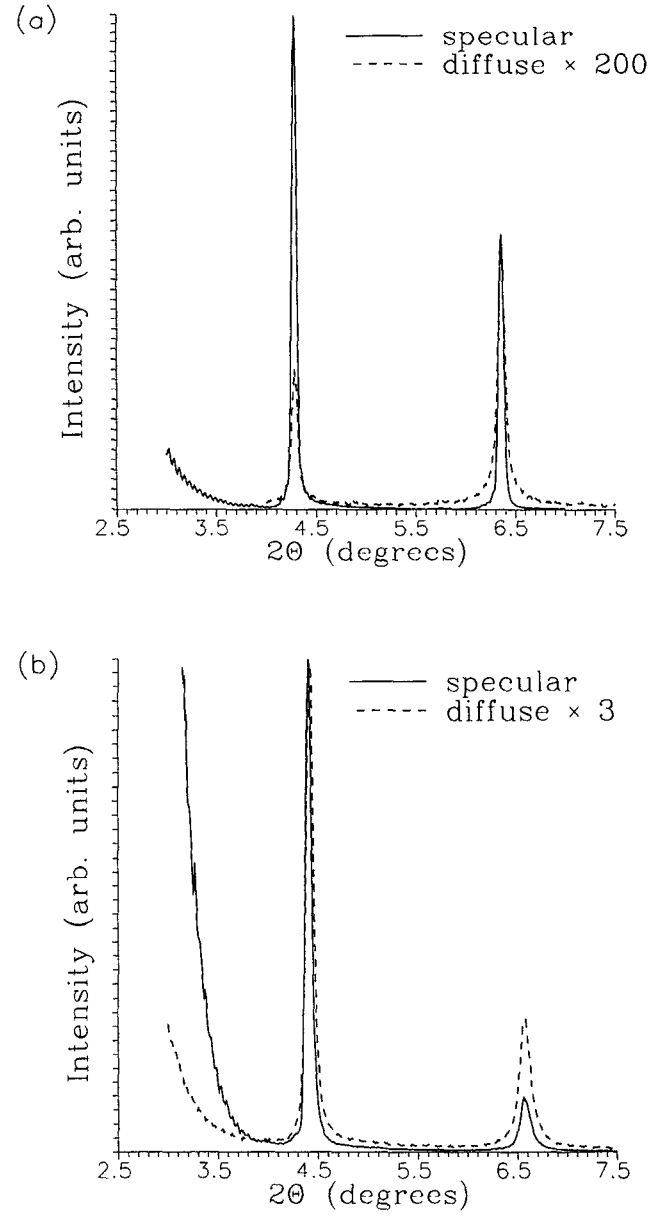

FIG. 5. Diffracted intensity for two geometries; $(\theta, 2\theta)$ scans (solid) and offset-$(\theta, 2\theta)$ scans with a 0.5° offset angle (dashed), through the second and third orders for 40-W/C layer-pair films deposited on different substrates, (a) Si(100), (b) fused silica. The figure shows that the diffuse intensity has the same S_z dependence as the specular intensity, but grows with increasing order relative to the specular intensity.

correlated roughness can be obtained from rocking curves. In Fig. 6, a series of rocking curves is plotted for the first through fifth orders for a 40-layer-pair mirror grown on Si(100). The curves show two components, a sharp central spike and a broad diffuse background with the diffuse component becoming relatively stronger with increasing order. The diffuse intensity again consists of components due to correlated and uncorrelated roughness. The diffuse intensity due to correlated roughness is peaked in the S_x, S_y plane at the Bragg condition. The vertically uncorrelated roughness will also produce a diffuse intensity in S_x, S_y that reflects its lateral correlation but, for equal amounts of correlated and uncorrelated roughness, this diffuse intensity will be weaker by a factor of $1/N$ than that due to the correlated roughness. Because the rocking curves are measured through the S_x, S_y plane at the Bragg condition, the shape of the diffuse intensity predominantly reflects the correlation in the x,y plane of the vertically correlated roughness, unless the uncorrelated part of the roughness is very much larger than the correlated part. The offset $(\theta,2\theta)$ curves shown in Fig. 5 verify that the diffuse reflectivity at the Bragg conditions ($S_z = 2\pi n/d$) is dominated by the vertically correlated roughness. The mag-

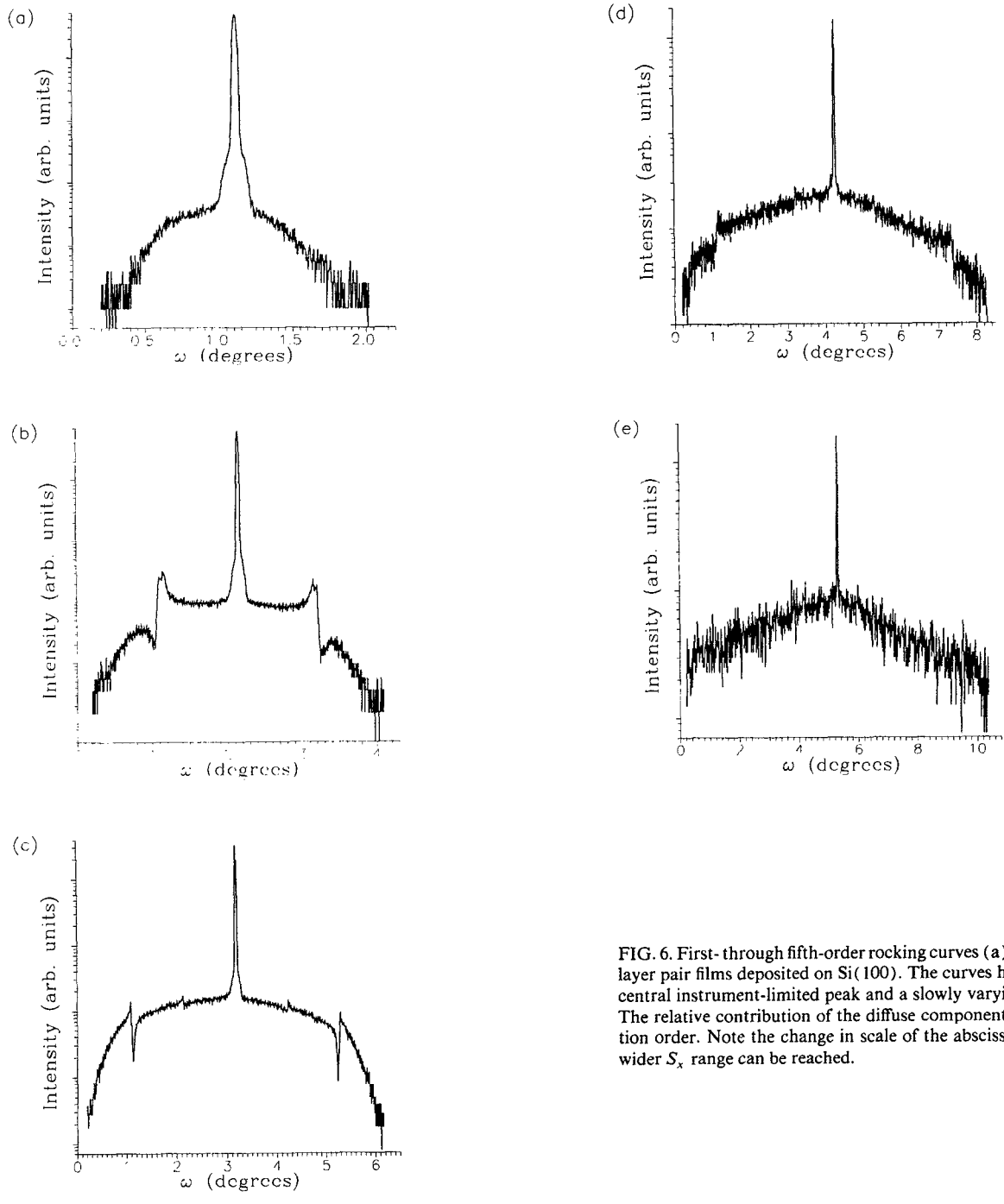

FIG. 6. First- through fifth-order rocking curves (a)–(e) obtained from 40-layer pair films deposited on Si(100). The curves have two components, a central instrument-limited peak and a slowly varying diffuse background. The relative contribution of the diffuse component increases with diffraction order. Note the change in scale of the abscissa. For higher orders, a wider S_x range can be reached.

nitude of the diffuse reflectivity due to uncorrelated roughness is reflected in the intensity measured away from the Bragg condition in S_z, which for these samples appears to be negligible.

Because the sample blocks respectively the incident or exit beam when ω approaches 0° or 2θ (the angle between the source and detector, which is fixed in a rocking measurement), the rocking curves can be taken only over the limited angular range of 2θ. This in turn limits the lateral correlation length scale that can be probed in reciprocal space to $S_x = \pm S_z \sin\theta = \pm 2\pi/l_{\text{limit}}$. The 10° angular range at the highest-order peak [see Fig. 6(e)] corresponds to a cutoff of lengths smaller than ~90°. At these limits there is still significant intensity, implying that lateral roughness correlations exist to a scale of less than 90°. This result is formalized in the next section where the model fits are presented.

Because the rocking curves are obtained at a grazing geometry the volume of the sample being probed is changing with the angle of incidence. This volume is proportional to its projected area, $A_0/\sin\omega$, and in kinematic diffraction theory the diffracted-beam intensity is proportional to the sample volume.[22] This leads to asymmetry in the rocking curves, with the low angles more intense than the high ones, as is observed. To remove this asymmetry, we multiply the measured rocking curves by $\sin\omega/\sin\theta$, which has the effect of normalizing the data to a constant sample volume.

Finally, we note that there exist satellite peaks in the diffuse background of the higher-order rocking curves. These arise at resonance conditions where the incoming or exit beam satisfies a Bragg condition and is doubly diffracted. We will return to a discussion of this effect in a later section.

1. Procedure for fitting the rocking curves

As stated above, the shape of the diffuse intensity in the I vs ω (rocking) curves reflects predominantly correlation of roughness in the x,y plane that is also correlated in z. The procedure used to fit the rocking curves involves the following steps. We begin by guessing a functional form for the correlation function $C(X,Y)$ and generating a theoretical profile in the same way as for single-surface roughness. This result is next multiplied by an envelope function that corrects for geometrical factors, which include beam attenuation and the effect of the cut through reciprocal space a rocking curve makes (it is not quite constant in S_z, which, for the case of correlated roughness, will cause an attenuation in the measured intensity at the extremes of the rocking curves). The profile is then convolved with a function representing the instrumental broadening, normalized to the peak intensity of the measured profile, and compared. The average roughness and the correlation length are varied to obtain the best fit. This procedure can be repeated for a new choice of the correlation function to improve the fit.

We have chosen to model the interfacial roughness in the same way as Sinha *et al.*[18] modeled surface roughness. Assume that for two points on a surface separated by some small distance $R = (X^2 + Y^2)^{1/2}$, the mean of the square of the difference in heights, $\langle [z(r) - z(r-R)]^2 \rangle$ increases proportionately to R^{2h}. This is known as self-affine roughness, where h is related to the fractal dimension, $D = 3 - h$. For $h = 1$, the surface height is varying relatively slowly. For smaller values of h, the surface is more jagged. For larger separations self-affine roughness diverges. This seems unphysical for a film of finite thickness. Therefore, the mean of the square of the height difference is chosen to approach a constant for large separations, the mean-square roughness σ.[2] A function that has these two limits is[18]

$$\{\langle [z(r) - z(r-R)]^2 \rangle\} = 2\sigma^2\{1 - \exp[-(R/\xi)^{2h}]\}, \tag{10}$$

from which the correlation function

$$C(R) = [\langle z(r)z(r-R) \rangle] = \sigma^2 \exp[-(R/\xi)^{2h}] \tag{11}$$

is obtained. Inserting values of $h = 1$ or $1/2$ into Eq. (11) gives the conventional forms for the correlation function that have been used to model visible-light scattering from rough surfaces. Differences due to the choice of h will appear in the shape of the diffuse component of the diffracted intensity. Reducing the value of h from 1 to 1/2 will put more of the diffuse intensity into higher angles while changing the FWHM of the diffuse function negligibly. Since the area under the diffuse curve increases with increased σ_c, a larger value of σ_c would be required in order to fit a curve with $h = 1/2$ than with $h = 1$ to account for the increased area at the higher angles.

Before discussing the two geometrical factors that affect the shape of rocking curves, we address whether the detector slits are long enough to integrate over an amount of the diffuse intensity sufficient so that they can be treated as infinitely long to reduce the problem to a one-dimensional one. This will, of course, depend in part on the lateral length scale of the roughness. The problem can be addressed by generating a profile that would correspond to that obtained with a point detector, i.e., from Eq. (4). This profile can be revolved and integrated over a finite range in S_y, mimicking the effect of a detector slit of finite length, and compared with the result obtained assuming an infinite slit length, e.g. from Eq. (7). For values of σ and ξ used in our fits the two results were equivalent, allowing us to use the simpler one-dimensional formulation.

The first geometrical factor to be accounted for in rocking curve fitting is the change in beam attenuation with ω that arises because the path length the x-rays travel is also changing. The change in path length is symmetric about the scan center and is depicted in Fig. 7. The longer path length at grazing incident and exit angles leads to a reduction of intensity at these extremes, causing the angular distribution of the diffuse scattering to be more sharply peaked than it would be if there were no attenuation. The magnitude of this effect can be estimated using kinematic diffraction theory. The change in intensity due to attenuation for an N-bilayer mirror of period d, at constant $S_z = S_z$ (Bragg) can be written:

$$F(2\theta,\omega) = \frac{\{1 + \exp[-N\alpha(2\theta,\omega)] - 2\exp[-N\alpha(2\theta,\omega)/2]\}}{\{1 + \exp[-\alpha(2\theta,\omega)] - 2\exp[-\alpha(2\theta,\omega)/2]\}}. \quad (12)$$

Here $\alpha(2\theta, \omega)$ is an attenuation coefficient that depends on 2θ and ω and is written:

$$\alpha\,\overline{(2\theta,\omega)} = [(\Gamma)\mu_W + (1-\Gamma)\mu_C] \times\{d\,[1/\sin(\omega) + 1/\sin(2\theta-\omega)]\}. \quad (13)$$

The term in square brackets is the average of the W and C linear x-ray absorption coefficients weighted by their relative layer thicknesses, where Γ is again the fraction of the bilayer spacing that is tungsten. The term in the curled brackets is the path length an x-ray travels in one bilayer. Equation (12), when multiplied with a term described next, is used as an envelope function with which to multiply the calculated rocking curves.

The second geometrical effect that must be accounted for when modeling rocking curve shapes is the geometry of the cut through reciprocal space. For perfectly correlated roughness the diffuse intensity is confined to planes parallel to the surface centered at the Bragg conditions. Because the rocking curve takes a radial cut in reciprocal space, the measured intensity will fall off with increasing value of $|(\omega - \theta)|$ as the detector deviates more and more from the S_x, S_y plane through S_z (Bragg). The S_z dependence of this intensity at any ω can be obtained from the $(\theta,2\theta)$ measurements at $\omega = 0$ and can be used to create a factor that corrects for this effect. The factor can be written

$$G(S_z) = I\,[S_z(\theta,\omega)]/I\,[S_z = S_z(\text{Bragg})]. \quad (14)$$

which has the effect of attenuating the intensity as S_z deviates from the Bragg condition. For a rocking curve, the value of S_z varies symmetrically about the scan center. Its 2θ and ω dependence can be written

$$S_z(\theta,\omega) = (2\pi/\lambda)[\sin\omega + \sin(2\theta-\omega)]. \quad (15)$$

This relationship can be used to map the intensity dependence of Eq. (14) into 2θ and ω variables.

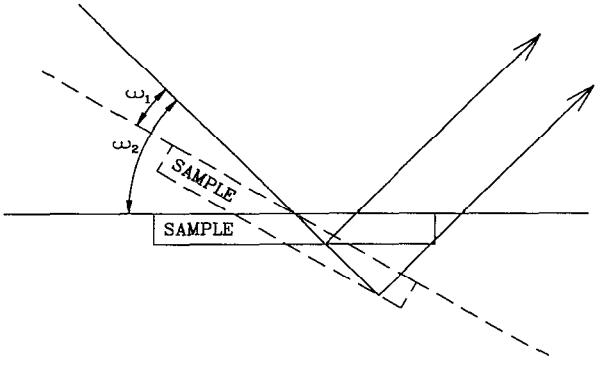

FIG. 7. Schematic diagram showing how the x-ray path length changes with the rocking angle, ω, during a rocking curve measurement. The reflection off the backsurface of the sample is shown.

To continue the calculation, the envelope function [a product of Eqs. (12) and (14)] is multiplied by the structure of a single interface, i.e., the single-surface result. Only the correlated roughness is included in this structure factor. The envelope function is sufficiently slowly changing so that it does not dominate the shape of the rocking curves near the scan center for the higher orders. This is essential, because the information we want to obtain is present in the structure factor of the single interface and a rapidly varying envelope would obscure it. The envelope functions for the third through fifth-order rocking curves are plotted in Fig. 8. We note that the envelope varies more slowly at higher orders and so at these orders it will affect the shape of the rocking curve less. Thus, higher-order rocking curves are more sensitive to the fit parameters.

Finally, the effect of finite instrumental resolution is included by convolving the theoretical curve with a function representing the instrumental broadening. An upper limit to the instrumental broadening is experimentally determined from the first-order rocking curve by subtracting the diffuse background, which is weak in any case for the first-order peak. This procedure gives a peak that has a full width at half maximum of $\sim 0.03°$. Convolving this function with the theoretical profile, which is a delta function plus a diffuse component, results in the sum of an instrument limited central spike and a diffuse component that is relatively unchanged because it is typically much broader than the instrument function. The main effect of the instrumental

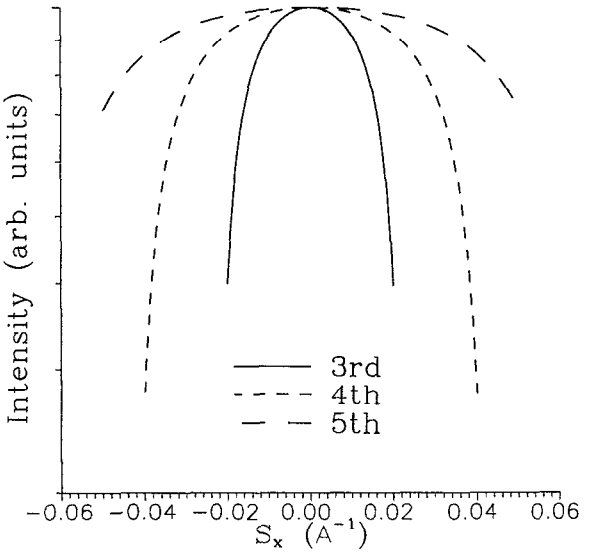

FIG. 8. Plots of the envelope function, the product of Eqs. (12) and (14), using mirror parameters $N = 40$, $d = 40$ Å, and $\Gamma = 1/2$ (a) for the third order, (b) for the fourth order, and (c) for the fifth order. Linear absorption coefficients of 12.2 cm^{-1} for carbon and 3300 cm^{-1} for tungsten (Ref. 25) were used to calculate the attenuation coefficient.

broadening for these measurements is to influence the ratio of the intensity of the central spike to the peak intensity of the diffuse component.

A second effect of instrument broadening is to limit the ability to resolve a lateral length scale of roughness larger than some length. For the above angular width and for a fifth-order rocking curve, this length is in the worst case on the order of micrometers. Because the instrument profile is much narrower than the diffuse component we measure, the length scale cutoff is much larger than the lateral correlation length of roughness present in the films. Such a cutoff would be important only in measurements of large-scale ($>\mu$m) figure error.

The features that were used to determine a good fit were: (1) the ratio of the peak intensities of the central spike and diffuse components, which depends on both σ_c and ξ, (2) the width of the diffuse component, which depends primarily on ξ, and (3) the overall shape of the diffuse component, which depends on the choice of the correlation function, i.e., on h. For a given value of h, a range of good fits can be found for various (σ_c, ξ) combinations. The error bars for the reported fits will reflect this uncertainty.

2. Correlated roughness

In Fig. 9, an example of a range of fits is shown for the fifth-order rocking curve of the 40-layer-pair film on Si(100) using $h = 1/2$ in the correlation function. The values of the parameters for the best fit are $\sigma_c = 1.9$ Å and $\xi = 35$ Å. The range of fits shows the relative uncertainty in σ_c and ξ for a given correlation function. Corresponding fits for the third and fourth orders of the 40-layer pair film grown on Si(100) are plotted in Fig. 10, again for $h = 1/2$.

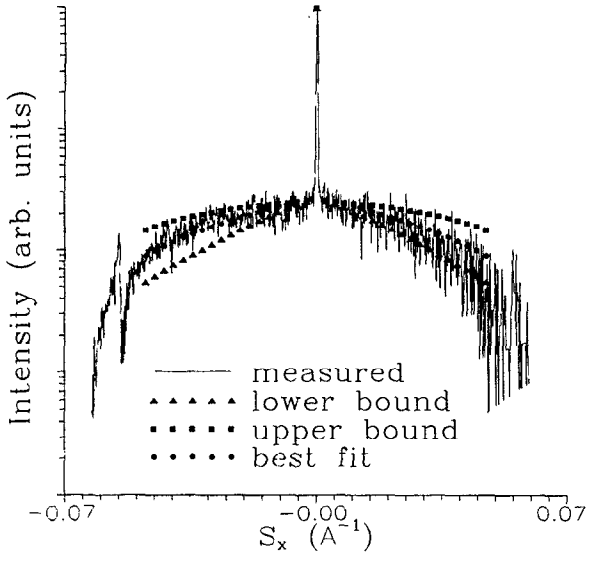

FIG. 9. The fifth-order rocking curve for 40 W/C layer pairs deposited on Si(100) (solid curve) and a range of calculated fits. The solid squares are obtained using $h = 1/2$, $\sigma_c = 2.2$ Å, and $\xi = 20$ Å, the solid triangles using $h = 1/2$, $\sigma_c = 1.7$ Å, and $\xi = 50$ Å, and the solid circles, and best fit, using $h = 1/2$, $\sigma_c = 1.9$ Å, and $\xi = 35$ Å.

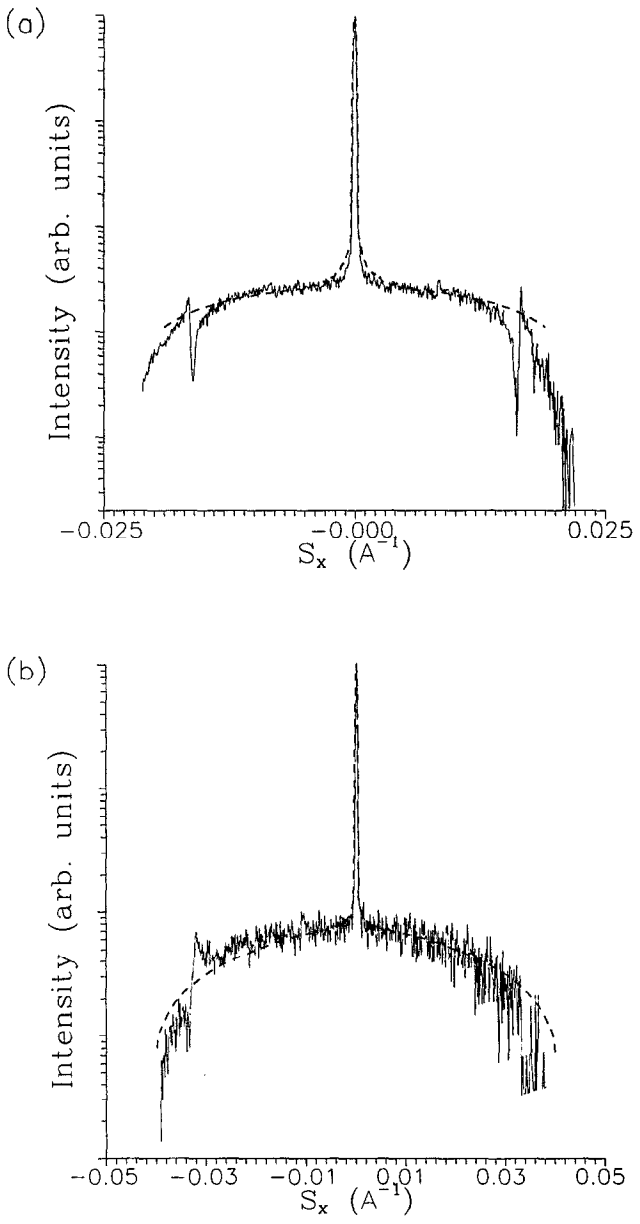

FIG. 10. Third- and fourth-order rocking curves for 40 layer pairs deposited on Si(100) and calculated fits using $h = 1/2$, $\sigma_c = 1.7$ Å, and $\xi = 35$ Å. (a) the third order, (b) the fourth order.

Best-fit values of $\sigma_c = 1.7$ Å and $\xi = 35$ Å were obtained for both orders, in good agreement with the fifth-order fit. The second-order fit parameters were the same as for the third and fourth. Given that essentially a single set of parameters can be used to fit the second through fifth orders gives confidence in the modeling and justifies the assumption that vertically correlated roughness is Gaussian distributed in z. It also suggests that for this sample the correlated roughness is not changing significantly as a function of depth (lower orders are more surface sensitive).

A value of $h = 1$ could also be used to fit the rocking curves, giving a smaller value for σ_c, $\sigma_c = 1.0$ Å, and the same value for ξ, $\xi = 35$ Å, although the overall fit was not as good. With a choice of $h = 0.2$ a fit was not achievable.

a. Dependence on substrate. It is reasonable to expect that changing the substrate material will affect predominantly the correlated roughness. From the specular reflectivity results [Sec. IV. (A)], it was found that the 40-layer-pair mirror deposited on fused silica had a relatively greater total roughness, $\sigma_{\text{tot}} = 6.6$ Å, than that for the equivalent mirror deposited on Si(100), $\sigma_{\text{tot}} = 3.4$ Å. This difference can be attributed almost entirely to differences in the correlated roughness, as will be shown here. The best fit for the third-order rocking curve for forty layer pairs deposited on fused silica is plotted in Fig. 11. Using $h = 1/2$, the best fit parameters were $\sigma_c = 5.6 \pm 0.5$ Å and $\xi = 1890 \pm 80$ Å. The uncorrelated roughness can be estimated using Eq. (7) and is of the same order for each mirror, $\sigma_u \sim 3$ Å. The simplest explanation is that substrate roughness is replicated by the deposited overlayers. Another possibility is that changing substrate material will affect how the initial layer nucleates. This change in the initial layer formed could then be replicated during the rest of the growth.

It is interesting to note that the lateral correlation length is much greater for the film grown on fused silica. Again one might expect that this difference arises from differences in the substrate roughness, although we have no direct evidence at this time. Such a difference should be observable on the substrates. Initial work measuring the roughness of Si(100) wafers using scanning tunneling microscopy (STM) gives values for the roughness parameters consistent with the values obtained from the rocking curves, including a reasonable agreement with the correlation function using $h = 1/2$.[23] Additional work is being performed on fused silica substrates covered with a thin conducting coating so that STM can be used.

b. Dependence on layer number. Correlated roughness appears to be relatively unchanged by increasing the number of layers deposited. The values for the correlated rms roughness ranged from a low of $\sigma_c = 1.4$ Å to a high of $\sigma_c = 2.3$ Å for layers deposited on Si(100). This range is most likely attributable to variations in substrate roughness and is consistent with the range of values for substrate roughness obtained from STM scans on Si(100).[23]

Additional evidence that the correlated roughness is relatively independent of the number of deposited layers is found from the order dependence of the fit values. For all films only small changes in the parameters were needed to give reasonable fits for the second through highest orders.

The results of the rocking-curve fitting for all samples along with estimates of the uncorrelated roughness are summarized in Table II. The values of the uncorrelated roughness were derived using the lower-limit values for σ_{tot} and so also represent lower limits.

We make two main observations from these data. The first is that the lateral correlation length of the propagated roughness can be quite short, as little as 20–60 Å for the films grown on Si(100), suggesting that assumptions treating fine-scale roughness as uncorrelated from layer to layer are not justified at least for this length scale. The second is that the contribution of the correlated roughness to the total roughness can exceed that of the uncorrelated part. Even for our best mirrors they are comparable. For ones deposited on silica, the correlated roughness dominates.

C. Rocking-curve satellites

In all rocking curves of order greater than the first, we observe extra peaks (or valleys) spaced symmetrically about the central peak. The strongest of these occurs when either the incident or exit beam satisfies the first-order Bragg condition, i.e., θ (incident or exit) $= \sin^{-1}(\lambda/2d)$. For rocking curves of order greater than 2, additional peaks are observed at positions corresponding to the second-order Bragg condition. These were relatively weaker. The presence of these satellites can be understood in terms of double diffraction. Because the intensity of the diffracted beams can be quite strong, ($\sim 60\%$ of the incident beam for the first-order peak) double diffraction must be included. In Fig. 12, we show the Ewald construction for a second-order rocking curve somewhere in S_x off the exact Bragg condition while the incident beam satisfies as well the exact first-order Bragg condition. A subsequent scattering of the first-order diffract-

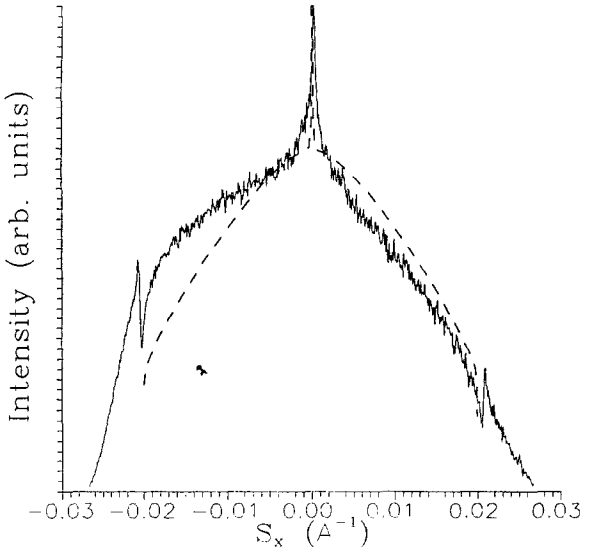

FIG. 11. The third-order rocking curve for 40 layer pairs deposited on fused silica and the calculated fit using $h = 1/2$, $\sigma_c = 5.6$ Å, and $\xi = 180$ Å.

TABLE II. Roughness and correlation length for several mirrors. The values of the correlated interfacial roughness, σ_c, and lateral correlation length, ξ, are from fits to rocking curves using $h = 1/2$ in Eq. (10). The values for the uncorrelated roughness are determined from Eq. (7) using the values for total roughness shown in Table I.

Sample	σ_c (Å)	σ_u (Å)	ξ(Å)
Fused silica substrate			
$N = 40$	5.6 ∓ 0.2	3.5	180 ∓ 40
Si (100) substrate			
$N = 40$	1.7 ∓ 0.3	2.9	$30 - 20/+30$
$N = 60$	1.5 ∓ 0.2	3.3	70 ∓ 20
$N = 80$	2.3 ∓ 0.3	3.8	50 ∓ 20

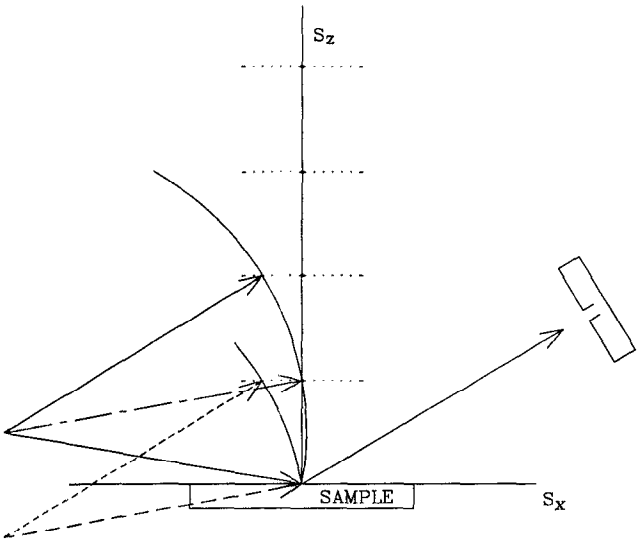

FIG. 12. Ewald construction for a second-order rocking curve at a resonance condition. The solid arrows show the diffraction geometry for the second-order peak at a value of S_x away from the central peak. For this angle of incidence, the first-order diffraction condition is exactly satisfied (dot-dashed arrow). This reflection is strong and the diffracted beam can be scattered again. This scattering is shown in reciprocal space by translating the dot-dashed curve to the origin (dashed arrow) and drawing a new Ewald sphere; which crosses the first-order reflection at a value of $S_x \neq 0$ (dotted arrow). The exit angles of the dotted and solid arrows are the same; hence both features appear in the detector at this specific angle.

ed beam is possible. The figure shows that the scattered intensity due to both the singly scattered second-order and the doubly scattered first-order beams leave the sample at the same angle, the angle at which the leftmost satellite occurs. The interference of these two beams gives the extra feature at this diffraction condition. Similar resonances have been observed for rocking curves measured on single surfaces.[18] Here the resonances occur when the incident or exit angle satisfies the critical angle for total external reflection. A dynamical diffraction model will be needed to fit the detailed shape of the rocking curves near the resonance conditions. We are attempting to make such calculations.

V. DISCUSSION

The results of the correlated-roughness analysis lend insight into the mechanisms of film growth for the *W/C* system. The result that the correlated roughness remains relatively constant throughout the film thickness suggests that the films are neither smoothening nor roughening appreciably on the lateral length of the correlated roughness, ξ. In other words, an initial perturbation present in the substrate or arising from the first deposited layer neither damps out nor grows during the deposition for our near-room-temperature conditions. This suggests that the lateral diffusion length of the deposited atoms is of the order of or less than the lateral correlation length. On the other hand, any trend in the increase in uncorrelated roughness is weak and certainly nowhere near that predicted by random filling (Poisson statistics), $\sigma = t^{1/2}$, where t is the total film thickness. Therefore, some lateral diffusion of adatoms must be occurring. The degree of diffusion and level filling can probably be predicted by fitting the results to rate equation models of the growth.[4]

Correlated roughness in these films will have an impact on their applicability for various soft x-ray optical elements. Correlated roughness leads to a relatively strong diffuse halo around the specular beam. How much of an effect it will have on imaging applications will depend in part on the wavelength being imaged and the lateral scale of the correlated roughness. A small value for ξ should prove beneficial as it spreads the diffuse intensity into a large angle, thus reducing its contribution near the specular direction. If the lateral correlations are much smaller than the wavelength of the scattered radiation, they will not contribute to the diffuse reflectivity. It should be noted that correlations exist over a larger length scale than ξ. The length ξ represents the $1/e$ value for the correlation function used. From the samples we measured ξ ranged from 20 to 200 Å, and so the correlated roughness will play an important role in optical elements designed for use in this wavelength range. It will be necessary to characterize the mirrors at wavelengths at which they will be used. We are pursuing such work.[24]

VI. SUMMARY

We have presented a method using x-ray diffraction by which the contribution of correlated roughness to the total interfacial roughness for multilayered thin films can be extracted. The method entails fitting the shape of rocking curves, collected with a narrow detector aperture, with a kinematically derived interface structure factor. From this fitting the magnitude and lateral correlation length of the correlated roughness is extracted. By using the traditional approach of modeling specular reflectivity, we obtain as well a value for the total interfacial roughness.

We have examined a series of W/C soft x-ray mirrors using this method. We find that roughness correlations are present to a significant extent on all samples. In addition, the lateral length scale of the correlated roughness can be surprisingly small. In our samples it ranged from 20 to 200 Å. We find, as might be expected, that the choice of substrate is important in determining the degree of correlated roughness. However, the correlated roughness appears to be independent of film thickness. Both the C and the W layers show no sign of crystallinity, suggesting that the deposition can be modeled with atoms more or less sticking where they hit, but with some short-range lateral diffusion (i.e. atoms falling into the nearest lattice site). The substrate roughness is then replicated quite precisely but there are additional random fluctuations in thickness. It will be interesting to compare films deposited at higher temperatures at which diffusion should become more significant.

This method of determining interfacial roughness correlations is applicable to any multilayer films that have enough difference in their layer structure factors to provide a diffracted beam. It may therefore be useful in checking roughness in such other classes of materials as heteroepitaxial multilayers for optoelectronic devices, metallic superlattices, or semiconductor-insulator composites.

ACKNOWLEDGMENTS

This work was supported in part by NSF Grants, DMR 89-18927 and 86-15089. N. S. acknowledges salary support for approximately fifteen months from the NSF Engineering Research Center for Plasma Aided Manufacturing. We thank M. Winokur and R. Matyi for useful discussions, and R. Matyi for providing us with computer programs for calculating $(\theta,2\theta)$ curves.

[1]For an overview of multilayers for x-ray optics, including the effect of interfacial roughness, see T. W. Barbee, Jr., SPIE **563**, 2 (1985).
[2]R. J. Noll, Opt. Eng. **19**, 249 (1980).
[3]R. Kariotis, J. Phys. A **22**, 2781 (1989).
[4]R. Kariotis and M. G. Lagally, Surf. Sci. **216**, 557 (1989).
[5]J. M. Eastman, in *Physics of Thin Films, Advances in Research and Development*, edited by G. Hass and W. R. Hunter (Academic, New York 1978), Vol. 10.
[6]C. K. Carniglia, Opt. Eng. **18**, 104 (1979).
[7]J. M. Elson, J. P. Rahn, and J. M. Bennett, Appl. Opt. **19**, 669 (1980)
[8]W. P. Zmek, J. E. Harvey, and E. C. Moran, SPIE **1160**, 217 (1989).
[9]J. E. Harvey, W. P. Zmek, and E. C. Moran, SPIE **1160**, 209 (1989).
[10]T. Ishikawa, A. Iida, and T. Matsushita, Nuc. Instrum. Methods Phys. A **246**, 348 (1986).
[11]A. Hornstrup, F. E. Christensen, J. L. Wood, M. Bending, and H. W. Schnopper, SPIE **984**, 174 (1988).
[12]A. M. Hawryluk, N. M. Ceglio, and D. G. Stearns, J. Vac. Sci. Technol. B **6**, 2153 (1988).
[13]H. Berrouane, J. M. Andre, C. K. Malek, S. Fouchet, F. R. Ladan, R. Rivoira, and R. Barchewitz, SPIE **1160**, 280 (1989).
[14]T. W. Barbee, Jr., J. C. Rife, W. R. Hunter, R. J. Cruddace, and P. Pianetta, SPIE **1160**, 636 (1989).
[15]D. G. Stearns, J. Appl. Phys. **65**, 491 (1988).
[16]B. G. Peterson, L. V. Knight, and H. K. Pew, SPIE **563**, 328 (1985).
[17]S. R. Andrews and R. A. Cowley, J. Phys. C **18**, 6427 (1985).
[18]S. K. Sinha, E. B. Sirota, S. Garoff, and H. B. Stanley, Phys. Rev. B **38**, 2297 (1988).
[19]E. L. Church and P. Z. Takacs, SPIE **1160**, 323 (1989).
[20]D. L. Rosen, D. Brown, J. Gilfrich, and P. Burkhalter, J. Appl. Cryst. **21**, 136 (1988).
[21]M. Born and E. Wolf, *Principles of Optics* (Pergamon, New York, 1983).
[22]R. W. James, *The Optical Principles of the Diffraction of X-rays* (Oxbow, Woodbridge, CO, 1982).
[23]D. E. Savage, J. Kleiner, N. Schimke, Y-. H. Phang, and M. G. Lagally (unpublished).
[24]N. Schimke, Y. -H. Phang, J. R. Jacobs, and M. G. Lagally (unpublished).
[25]B. D. Cullity, in *Elements of X-ray Diffraction* (Addison-Wesley, Menlo Park, CA 1967), p. 467.